Journal of Physics: Conference Series

Measuring three-dimensional deformation with surface-imaging ORVIS

To cite this article: M A Cooper *et al* 2014 *J. Phys.: Conf. Ser.* **500** 182008

IOP Publishing
doi:10.1088/1742-6596/500/18/182008

Measuring three-dimensional deformation with surface-imaging ORVIS

M A Cooper, P E Specht and W M Trott

Explosives Technologies Group, Sandia National Laboratories, Albuquerque, NM, 87185-1454, USA

E-mail: `macoope@sandia.gov`

Abstract. With growing interest in understanding heterogeneous material phenomena under shock compression and the advancement of computational methods, three-dimensional data suitable for model validation and scientific pursuit is needed. The optically-recording velocity interferometer system (ORVIS) is a velocity interferometer that measures the apparent motion of a set of parallel interference fringes. Initially demonstrated for collecting one-dimensional data at a point using a streak camera and a focused laser spot, line-imaging ORVIS is a useful extension for the collection of two-dimensional data using a streak camera and a laser light sheet. We extend ORVIS operation further to a surface-imaging mode for collecting three-dimensional data using a framing camera and an expanded region of laser illumination. In surface-imaging mode, snapshots of surface velocity across a cross-sectional area are collected at regular time intervals and combined to yield the surface velocity history. Surface-imaging ORVIS is demonstrated through an analytical model of a vibrating circular membrane and an experimental and analytical model of a rotating ellipse. A discussion of the analysis methodology and some experimental challenges are discussed.

1. Introduction

The Optically-Recording Velocity Interferometer System (ORVIS) is a velocity interferometer that measures the apparent motion of a set of parallel interference fringes. The diagnostic has routinely been applied to planar impact tests in gun facilities and studies of shocks in a variety of materials [1–7]. In all applications, the diagnostic collects Doppler shifted laser light from a moving target; this signal is processed by a velocity interferometer and the resulting interference fringe pattern is recorded optically by a camera. An illustration of the diagnostic using a Michelson interferometer coupled to a moving target is given in figure 1. The inlet beam from the laser contains optics for the desired target illumination. When operated exclusively in Line-Imaging ORVIS (LIO) mode, a light sheet is projected onto the target by a combination of one spherical and three cylindrical optics [5]. When operated in Surface-Imaging ORVIS (SIO) mode, an expanded laser spot is projected onto the target by a single spherical lens. Lenses L1, L2, L3 collect the return light and produce a magnified image of the target. After the interferometer, the superimposed fringe pattern at redundant recombination planes (R1, R2), is imaged through the slit of a streak camera for LIO or at a CCD/intensifier for SIO (figure 2). LIO has already been shown to exceed the spatial resolutions of existing multi-point diagnostics in one dimension and thus, SIO has the potential to exceed the available spatial resolutions of an array of multi-point diagnostics in two dimensions.

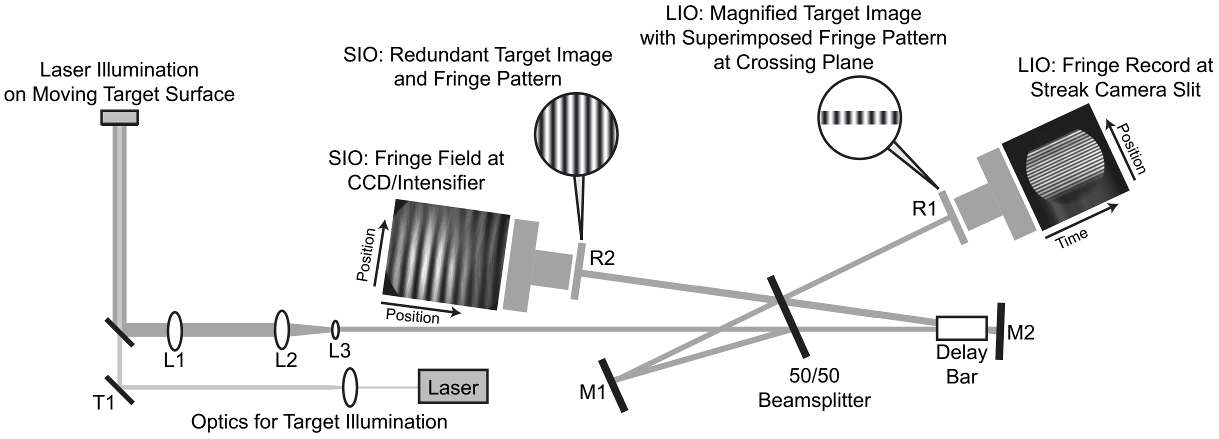

Figure 1. Diagnostic arrangement for LIO and SIO operation.

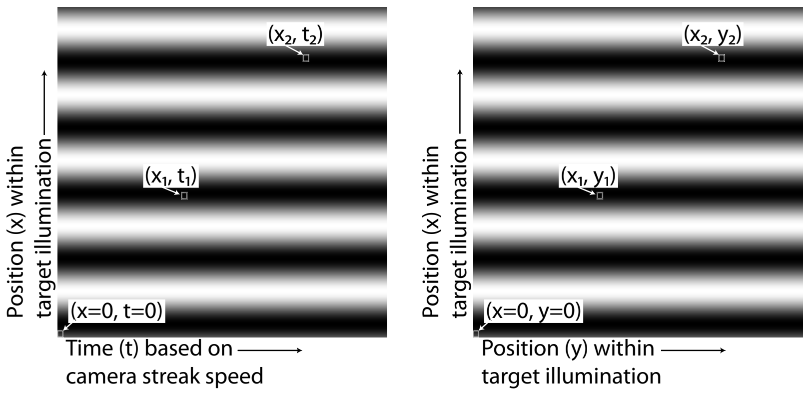

Figure 2. Fringe record details: (left) LIO in terms of x-position within target illumination and time imaged at a specific y-position on target; (right) SIO in terms of x- and y- position within target illumination imaged at a specific time with finite exposure.

SIO records stop motion images of the fringe field at discrete times. The earliest demonstration of SIO was conducted on a laser-driven flyer launch in which only one frame was collected per test due to camera technology limitations [3]. However, given a camera with a sufficiently fast interframe time relative to the target motion under observation, multiple images from a single test can be correlated to determine the evolution of velocity in two-dimensional space. The change of phase from a baseline image is evaluated for each image pixel using rolling quadrature or FFT analysis methods as in LIO.

2. Analytical example of vibrating membrane

The wave response of a vibrating circular membrane with zero boundary conditions is calculated for multiple time steps and is used to demonstrate the mechanics of SIO image analysis. The MATLAB® calculations solve for the membrane velocity assuming radial symmetry, $V(r,t)$. The results are remapped into Cartesian coordinates, $V(x,y)$, and velocity is converted into pixel intensity, $I(x,y)$, given a background fringe frequency, ω, and velocity-per-fringe constant, VPF.

$$I(x,y) = \sin[2\pi\omega x + V(x,y)/\mathrm{VPF}] \tag{1}$$

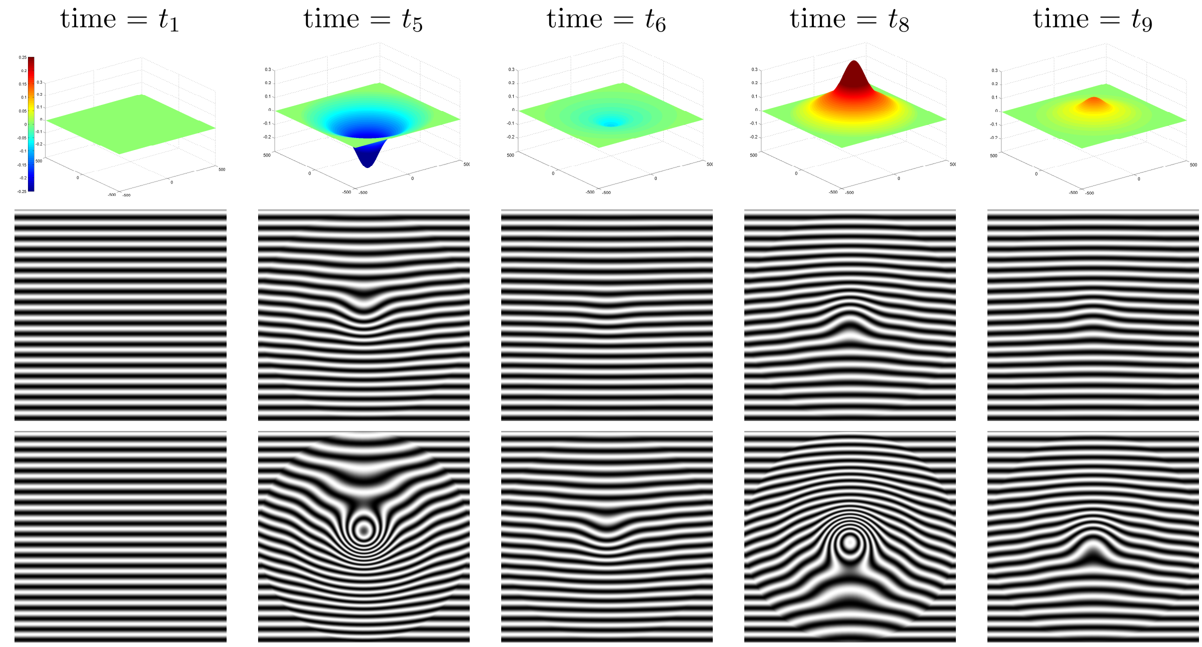

Figure 3. Analytical example of vibrating membrane with full field velocity and fringe records presented at five random times. (Top row) calculated velocities, $V(x, y)$; (Middle row) full field fringe record assuming VPF = $V_{max}/2$; (Bottom row) full field fringe record assuming VPF = $V_{max}/8$.

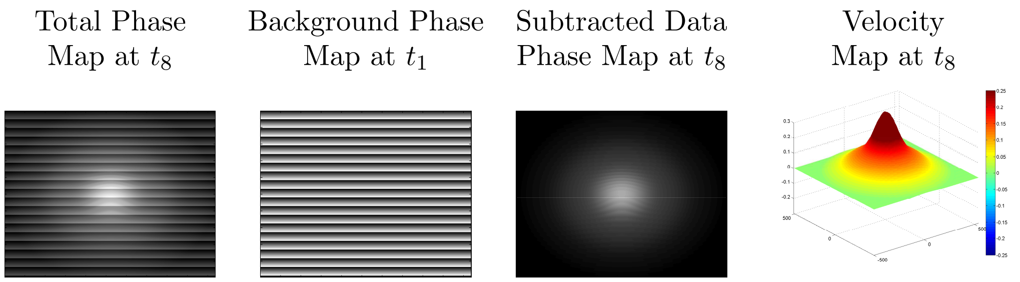

Figure 4. Velocity map calculation utilizing full field fringe records at time t_8, with surface motion, and time t_1, with no surface motion.

The calculated membrane velocity at all (x, y) positions is shown in the first row of images in figure 3 for five random time steps. The center region is observed to oscillate about a baseline position with no motion at the image boundaries. The second and third rows of figure 3 show the calculated full field fringe records for two different values of the interferometer velocity-per-fringe constant (VPF = $V_{max}/2$ and $V_{max}/8$). The image analysis in SIO proceeds in the same fashion as is common for LIO by comparing the data image at a particular time to a baseline image with no motion. The phase map corresponding to the change in velocity from the no-motion baseline phase map is determined using the rolling quadrature or FFT analysis methods. Once the background phase has been subtracted, velocity is calculated using the VPF constant as illustrated in figure 4.

For surface velocities less than or equal to the VPF constant there should be no need to reconcile fringe jumps. For surface velocities greater than the VPF constant, it is possible for the fringe record to show isolated rings (as is the case for the bottom row of figure 3) or for fringes to appear or disappear at certain image locations. In these cases, the methodology to add fringe jumps in (x, y) space to reconcile these discontinuities can become very challenging and at best manually cumbersome.

3. Sinusoidal motion from a rotating ellipse

To experimentally demonstrate the SIO diagnostic, a benchtop experiment utilizing a rotating aluminum ellipse was constructed (left image of figure 5). The rotation of an ellipse can be numerically modeled, enabling verification of the experimentally measured velocities. The interference fringe pattern during rotation was imaged 102 times with a Shimadzu HPV-2 high-speed camera at a rate of 32,000 frames/s and an exposure time of 3.9 μs. The VPF equaled 100 m/s, which was the lowest VPF possible given the interferometer dimensions. The ellipse was rotated at speeds around 25,000 rpm, which, given its major and minor diameters, corresponded to peak velocities in the direction of laser illumination of approximately 30 m/s. The rotation speed was measured in each experiment with a laser diode and photodetector (left image of figure 5). The surface curvature of the ellipse reflected much of the laser light outside of the collection optic. To improve light collection at the first collection optic, the 6.35-mm-thick edge of the ellipse was roughened with sandpaper to generate a more diffuse reflection.

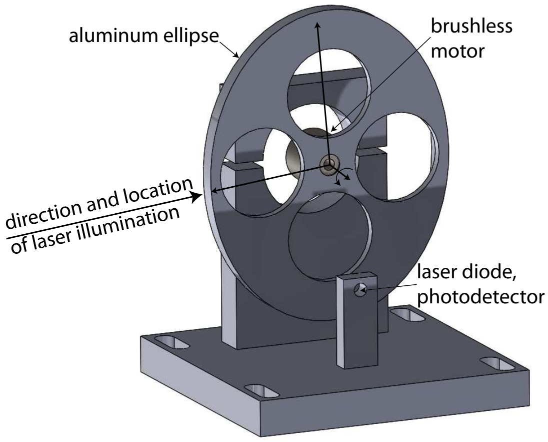

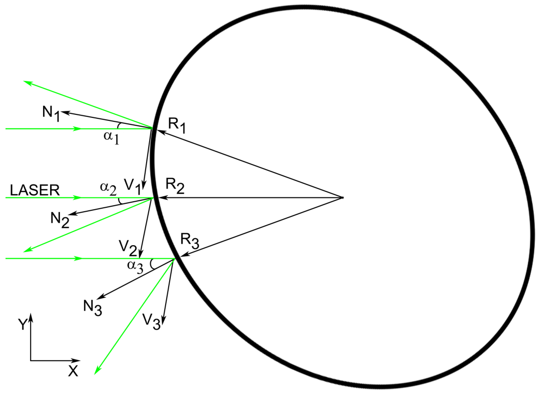

Figure 5. (Left) Illustration of the rotating ellipse experiment for monitoring surface motion with SIO. (Right) Schematic of inlet laser light and its reflection from different points within the incident laser spot on the edge of the rotating ellipse. Velocity vectors are illustrated for ellipse rotation about the $+z$-axis.

Experimental fringe patterns obtained for the ellipse along with the corresponding velocity profiles are shown in figure 6. The velocity surface maps clearly show a variation in velocity over the finite measurement area of the beam. This variation is due to the surface curvature of the ellipse, which causes every point within the beam to have a different velocity vector. This is schematically illustrated in right image of figure 5. This curvature also means the interferometer actually measures an apparent velocity V_a based on the x and y components of the velocity vector.

$$V_a = 1/2V_x(\cos(2\alpha) + 1) + 1/2V_y \sin(2\alpha) \quad (2)$$

Here, V_x and V_y are the components of the velocity vector at a given point and α is the angle formed between the incident beam and the surface normal.

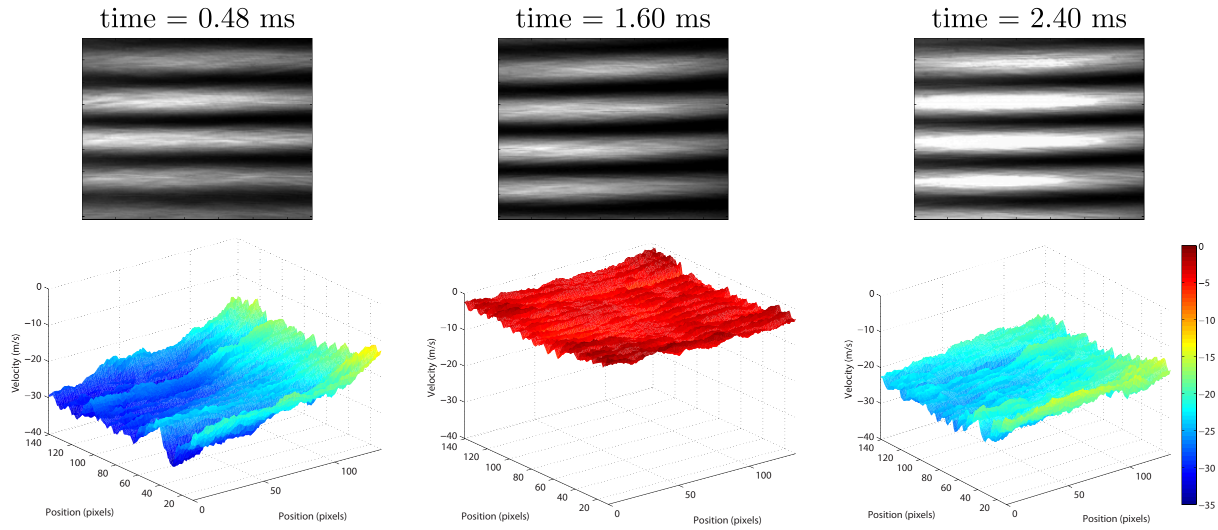

Figure 6. Full field fringe records and velocity surface maps at three times measured from the rotating ellipse.

The apparent velocities over the area of the incident laser beam are averaged together to obtain a single velocity versus time record for the experiment. This was also done numerically based on the experimental parameters and ellipse dimensions. A comparison of the experimental and numerical results is presented in figure 7 showing only rough agreement of the oscillation period and peak velocities. Some of the remaining discrepancies between the model and the experiment can certainly be attributed to experimental imperfections not numerically accounted for: variations in return light intensity due to surface curvature, low signal-to-noise ratio ($V_{max} \approx 0.1 - 0.3$VPF), large depth-of-field variations, vibration and run-out of the ellipse assembly, and misalignment of the laser beam to the axis of rotation. Efforts are ongoing to improve these experimental imperfections.

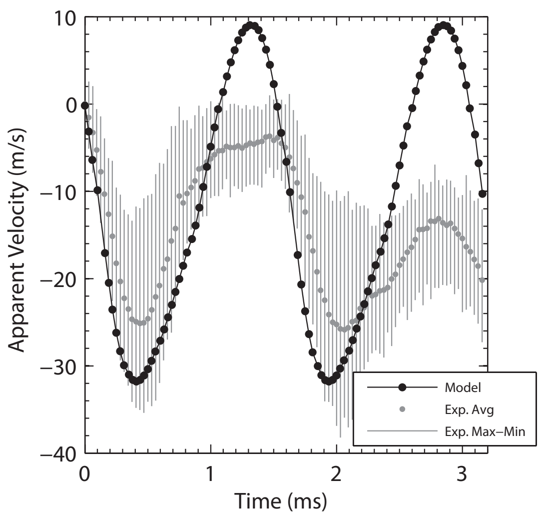

Figure 7. Comparison of analytically predicted and experimental apparent velocities versus time of ellipse rotation.

4. Conclusions

We have demonstrated surface-imaging ORVIS in two applications showing the versatility and potential usefulness of the diagnostic. The ability of the SIO to resolve the motion of the ellipse highlights its versatility when compared to other interferometers, such as Fabry-Perot velocimetry [8] or photonic Doppler velocimetry [9, 10], which are not able to resolve transverse motion. Ongoing efforts will be applying both LIO and SIO to upcoming experiments and conducting further analysis of the utility and limitations of ORVIS in detecting non-planar surface motion.

Acknowledgments
Adam Sapp is gratefully acknowledged for conducting the rotating ellipse experiments. Sandia National Laboratories is a multi-program laboratory managed and operated by Sandia Corporation, a wholly owned subsidiary of Lockheed Martin Corporation, for the U.S. Department of Energy's National Nuclear Security Administration under contract DE-AC04-94AL85000. Approved for unlimited release, SAND2013-9202C.

References
[1] Bloomquist D D and Sheffield S A 1983 *J. Appl. Phys.* **54** 1717
[2] Sheffield S A, Bloomquist D D and Tarver C M 1984 *J. Chem. Phys.* **80** 3831
[3] Trott W M, Castaneda J N, O'Hare J J, Knudson M D, Chhabildas L C, Baer M R and Asay J R 2001 *Fundamental issues and applications of shock-wave and high-strain-rate phenomena*. Staudhammer K P, Murr L E, and Meyers M A, Eds. Elsevier Science Ltd, Oxford. 647
[4] Celliers P M, Bradley D K, Collins G W, Hicks D G, Boehly T R and Armstrong W J 2004 *Rev. Sci. Instrum* **75** 4916
[5] Trott W M, Baer M R, Castaneda J N, Chhabildas L C and Asay J R 2007 *J. Appl. Phys.* **101** 024917
[6] Cooper M A, Trott W M, Schmitt R G, Short M and Jackson S I 2012 *AIP Conf. Proc.* **1426** 595
[7] Bolme C A and Ramos K J 2013 *Rev. Sci. Instrum* **84** 083903
[8] Goosman D R, Frank A M, Chau H H and Parker N L 1984 *27th Tech. Symp. Intl. Society of Optics and Photonics* 127
[9] Dolan D H 2009 *AIP Conf. Proc.* **1195** 589
[10] Briggs M E, Hull L M and Shinas M A 2009 *AIP Conf. Proc.* **1195** 577